Applied Energy 216 (2018) 588–601

Contents lists available at ScienceDirect

Applied Energy

journal homepage: www.elsevier.com/locate/apenergy

Performance and operational effectiveness of evacuated flat plate solar collectors compared with conventional thermal, PVT and PV panels

R.W. Moss[a,*], P. Henshall[b], F. Arya[c], G.S.F. Shire[a], T. Hyde[c], P.C. Eames[d]

[a] School of Engineering, University of Warwick, Coventry CV4 7AL, UK
[b] Oxford Brookes University, formerly Centre for Renewable Energy Systems Technology, Loughborough University, UK
[c] School of the Built Environment, University of Ulster, UK
[d] Centre for Renewable Energy Systems Technology, Loughborough University, UK

HIGHLIGHTS

- A high vacuum increases efficiency and reduces heat losses.
- Test results were in good agreement with theoretical models.
- 50% higher efficiency than conventional panels or tubes at T_M = 100 °C, G = 1000 W/m^2.
- 104% increase over conventional flat plate in predicted heat to district main operating at 85 °C.
- PVT panels are more effective than organic Rankine cycles for low temperature heat and power.

ARTICLE INFO

Keywords:
Evacuated
Flat plate
Solar
Collector
Organic Rankine cycle
Weather

ABSTRACT

The concept of an evacuated flat plate (EFP) collector was proposed over 40 years ago but, despite its professed advantages, very few manufacturers have developed commercial versions. This situation suggests both technical difficulties in manufacturing a competitively-priced sealed for life panel and a lack of awareness of the benefits of such panels.

This paper demonstrates an evacuated flat plate simulation that closely models experimental efficiency measurements. Having established the validity of the model, it compares published data for a commercial EFP collector with predictions for an optimal design to investigate whether any further efficiency improvement might be possible. The optimised design is then evaluated against alternative solar energy devices by modelling a number of possible applications. These comparisons should inform choices about solar options for delivering heat: EFP collectors are well-suited to some of these applications.

Evacuated flat plate collectors are a possible alternative to concentrating collectors for Organic Rankine Cycle power generation. The annual output for all the modelled collectors was found to be a quadratic function of delivery temperature: this enabled a novel optimisation of ORC source temperature. Predictions for concentrating and non-concentrating ORC plant are compared with a PV/thermal alternative. The ORC output is significantly less than a PV panel would achieve; applications needing both heat and power are better served by PVT panels. This is an original and novel result.

1. Introduction

1.1. Evacuated flat plate solar thermal collectors

Non-concentrating solar thermal collectors for low temperature applications such as domestic solar hot water (DSHW) conventionally adopt either a flat plate (FP) or evacuated tube (ET) format. Evacuated tube collectors can also be used for medium-temperature applications such as industrial process heat.

Of the UK's primary energy consumption approximately 26% is used for space heating [1]. The EU requirement for process heat in the 80–240 °C range has been estimated as 300 TWh per annum [2] and process heat is 38% of the US total energy use [3]. High efficiency solar thermal technologies can contribute to the decarbonising of these sectors.

Evacuated flat plate (EFP) solar thermal collectors are anticipated to

* Corresponding author.
E-mail address: r.moss@warwick.ac.uk (R.W. Moss).

https://doi.org/10.1016/j.apenergy.2018.01.001
Received 9 August 2017; Received in revised form 18 December 2017; Accepted 1 January 2018

Nomenclature

A_A	frontal area of absorber (m^2)
A_g	collector gross area (m^2)
C	effective heat capacity of absorber (J/m^2 K)
E_u	useful heat to absorber per time step (J/m^2)
E_1	annual heat output for absorber at temperature T_1 (Wh/m^2)
$E_{eq,Th}$	thermal equivalent of combined annual energy output (Wh/m^2)
G	total (beam + diffuse) irradiance (W/m^2) measured perpendicular to collector
G_{clear}	predicted irradiance, clear conditions (W/m^2)
G_E	effective irradiance, with beam component perpendicular to plate (W/m^2)
G_v	irradiance reference value (W/m^2)
I_{sc}	solar irradiance above atmosphere (W/m^2)
$\dot{Q}_u$	useful heat output (W/m^2)
$\dot{Q}_1$	heat output with absorber at temperature T_1 (W/m^2)
T_a	ambient temperature (°C)
T_g	cover glass temperature (°C)
T_p	plate mean surface temperature (°C)
T_{env}	environment radiative (sky) temperature (°C)
T_{HM}	heating main temperature (°C)
T_M	mean temperature difference $T_p - T_a$ (°C)
T_1, T_2	absolute temperatures of heat transferred into and out of a heat engine cycle (K)
$T_{1,opt}$	heat delivery temperature that maximises value of energy produced (K)
U_L	overall heat loss coefficient (W/m^2 K)
a,b,c	curve fit coefficients for heat output
a_0, a_1, k	standard atmosphere constants for mid-latitude climate
f	ratio of ORC to Carnot efficiency (second law efficiency)
f_d	fraction of radiation that is diffuse
h_i, h_o	heat transfer coefficient (W/m^2 K) to inward or outward-facing glass surface
k_τ	weather clearness index
q_{abs}	rate of heat absorption in glass (W/m^2)
t	time (seconds)
v	energy cost ratio, electricity:heat
$\alpha_1, \alpha_2, \alpha_3$	coefficients of efficiency polynomial
ε_{eg}	effective emissivity, environment to glass
ε_{pg}	effective emissivity, plate to glass
η_A	efficiency based on absorber area
η_g	efficiency based on gross area
η_{ORC}	Organic Rankine Cycle efficiency
$\eta_0, \tau\alpha$	transmission-absorbance product
λ	rate constant for exponential temperature step decay
μ	cycle profitability parameter $(v-1)f$
σ	Stefan-Boltzmann constant
τ_b, τ_d	beam and diffuse transmission coefficients for clear atmosphere

Subscripts and superscripts

‘	linearised parameters

Abbreviations

CHP	combined heat and power
DSHW	domestic solar hot water
EFP	evacuated flat plate collector
ET	evacuated tube collector
FP	flat plate collector (non-evacuated)
ORC	Organic Rankine cycle
PTC	parabolic trough collector
PV	photo-voltaic panel
PVD	physical vapour deposition
PVT	photo-voltaic/thermal panel
RTD	resistance temperature detector
TVP	evacuated flat plate collector by *TVP Solar*

combine the high fill factor, ease of cleaning and visual aesthetics of FP collectors with the low heat loss coefficient of ET collectors. They consist of a flat absorber contained within an evacuated enclosure with a top glass cover. An array of pins supports the glass cover against atmospheric pressure loading. Such collectors can achieve high operational temperatures suitable for many industrial applications and also operate efficiently in low irradiance conditions, a valuable feature for solar thermal collectors in the UK and at high latitudes. Unlike concentrating collectors, EFP collectors do not track the Sun; they can therefore be integrated into the building envelope, as the roof or fascia, where they can provide efficiency gains through building insulation [4,5]. The use of a façade to generate heat may also be valuable [6].

Two different designs of EFP collectors were built, each using a flooded panel absorber but with different enclosures. The test results are summarised here to demonstrate the accuracy of a simulation model: more comprehensive test details are given in Moss et al. [7]. Further simulations, of an improved design, have demonstrated the advantages for DSHW heating under typical UK irradiance conditions and assessed the potential use of an organic Rankine cycle for power generation.

1.2. Recent developments in thermal collectors

Much research has taken place over the past 20 years to improve efficiency in conventional solar collectors. Suman et al. [8] provides a detailed overview of solar collector technology and configurations whilst Colangelo et al. [9] reviews research into flat plate collectors over the past decade.

Collector efficiency is often characterised as $\eta = \tau\alpha - \frac{U_L T_M}{G}$ where T_M is the difference between absorber and ambient temperatures. An ideal high-efficiency collector would combine a transmission-absorbance product $\tau\alpha \approx 1$ with a low heat loss coefficient U_L and operate under high irradiance levels G. The optimisation of $\tau\alpha$ involves spectrally selective coatings and absorption media. Selvakumar and Barshilia [10] has reviewed the use of PVD coatings for medium and high temperature solar thermal applications. Colangelo et al. [11] tested the viability of nanofluids as selective absorbers. Anti-reflection coatings on the cover glass improve optical transmission: Caër et al. [12] developed a sol-gel technique for reducing the refractive index of SiO_2 to create a durable anti-reflection coating.

The absorber temperature is a key parameter in determining the choice of solar collector. Domestic solar hot water (DSHW) applications only require temperatures of order 70 °C but more novel applications such as industrial process heat, combined heat and power (CHP) or refrigeration require higher temperatures. Freeman et al. [13] investigated the suitability of thermal collectors for small scale CHP. Absorption refrigeration systems require heat at 70–120 °C [14]. Alobaid et al. [15] compared the merits of thermal collectors and PV panels to power solar cooling systems.

High temperature applications such as thermal power stations typically use concentrating collectors [16,17]: these minimise the efficiency penalty at high T_M by effectively increasing the irradiance intensity G. The insensitivity to diffuse radiation, complexities of the tracking and the need for regular mirror cleaning mean that they tend

to be used only for large open-air installations in dry climates, though Zou et al. [18] has proposed a domestic version for use in cold climates, Cohen and Grossman [19] built and tested a rooftop-mounted spherical mirror concentrator and Buttinger et al. [20] developed a low concentration, non-tracking trough collector. The latter's use of low pressure krypton greatly reduced the heat loss and approximately doubled the efficiency at $T_M = 100$ °C.

Wang et al. [21] describes a high efficiency combination of evacuated tube and concentrating rear reflector. Li et al. [22] evaluated the performance of a non-imaging concentrator plus evacuated tubes to supply heat for absorption chiller air-conditioning systems and Mwesigye and Meyer [23] compared three nano-fluids to improve heat transfer in a parabolic trough system. Qu et al. [24] built a 300 kW trough collector with altazimuth tracking.

An alternative approach for obtaining high efficiency at elevated T_M without the need for concentrating optics is to reduce both the radiation and conduction components of the heat loss coefficient U_L. The radiative part may be minimised using highly selective surface treatments, for which many options are available [10]. Meanwhile various approaches have been suggested to lessen the conduction component. Benz and Beikircher [25] examined the possibility of using a low pressure (1–10 kPa) to inhibit convection together with krypton to reduce the conductivity. Beikircher et al. [26] used a wide air gap to reduce conduction together with multiple intermediate glass or plastic films to inhibit convection. Ehrmann and Reineke-Koch [27] used a double glazed cover glass. Brunold (SPF) [28] describes a prototype collector using stacked 7 mm diameter glass capillary tubes as a thick transparent insulating layer that inhibits convection.

The use of a vacuum to eliminate conduction losses in a flat plate collector, in particular, has been studied by Benz and Beikircher [25] and Benvenuti and Ruzinov [29–31]. Conductivity in a gas is not a function of pressure until at low pressures the molecular mean free path exceeds the characteristic separation of the enclosure surfaces; beyond this point the heat transfer coefficient between surfaces is proportional to pressure but independent of the surface spacing [7].

Two evacuated flat plate collectors are available commercially. The SRB design [29] uses a long, thin format (64 cm wide, up to 3 m long) with an internal metal framework. The front and back glass covers are supported by longitudinal ribs; the absorber uses copper strips that sit between the ribs and are welded to a stainless tube.

The TVP design [32,33] uses low melting point frit glass to seal the cover glass to a NiFe alloy edge spacer with a stainless steel back cover. The similarity in expansion coefficients between glass and this 48% nickel alloy avoids the shear stress peaks described by Henshall et al. [34]. The glass is supported by pillars passing through holes in the absorber.

Many proprietary details of these commercial collector designs are however undocumented. The present investigation into theoretical and practical aspects of EFP collectors is intended to provide definitive data to guide future evacuated flat plate collector designs. A novel comparison with alternative panels aims to inform installation choices and policy decisions in the quest for a low-carbon future.

2. Manufacture and instrumentation of evacuated collectors

2.1. Enclosure styles

Two styles of collector were developed: they share a common absorber design, mounted in different enclosures. In each case an array of pillars supports the cover glass against the atmospheric pressure load.

The "tray" style of enclosure uses a stainless steel tray with a single cover glass on the front [7,34]. This concept is intended for industrial process heat applications where the visual appearance of the back face is not architecturally significant.

The "symmetrical" enclosure, Fig. 1 and Table 1, resembles a vacuum double glazing panel in that it has a sheet of glass to the rear as well as the front. The U-value is almost as low as for a vacuum glazing panel and the glass rear face makes its appearance suitable for architectural use in a building façade; it combines thermal insulation, heat collection and solar shading.

The results presented here were taken from the symmetrical enclosure test using water with a corrosion inhibitor additive. Results for the tray enclosure and further experimental details are given separately in Moss et al. [7].

Approximately 3% of the absorber area was taken up by the 49 through holes, so only 97% of the "absorber area" actually absorbs heat. The ratio of absorber area/gross area was 68.3%; this is lower than the typical 89% for commercial flat panels because the latter are typically 2 m^2 or more in area as well as having narrower edges (13–35 mm, [35]). Full size evacuated flat panels would not be expected to suffer a significant fill factor penalty relative to conventional panels.

2.2. Absorber manufacture

2.2.1. Configurations and coatings

Following initial investigations [36] into micro-channel and serpentine tube absorbers a flooded design of absorber was chosen. 0.7 mm T316 stainless steel sheets are hydro-formed and TIG welded to a 0.9 mm baseplate [37]. An array of through holes allows the glass support pillars to pass through the absorber without making contact, Fig. 2. The internal height is typically 2 mm, increasing to 3.5 mm near the intake and outlet connections.

Having eliminated gaseous conduction losses, the main heat loss mechanism is radiative transfer between absorber and cover glass. Many selective emissivity coating options were investigated including commercial solar panel coatings, black solar panel paint (Solkote®), black nickel [38,39] and black chrome plating, sol-gel [40] and PVD coatings [10,41].

Commercial coatings after many years' development now offer emissivities as low as 0.04. Four manufacturers were approached but none were able to apply their coatings on a one-off basis to a welded steel absorber.

Black chrome plating was widely adopted as a spectrally-selective surface for solar panel use in the 1970s [42]. Two local black chrome suppliers were used. Chromium plating suffers from a highly non-linear relationship between electric field strength and deposition rate: in trials it proved very difficult to obtain a sufficiently uniform coating, particularly when moving from small samples to the full size absorber. The coating typically achieved an absorbance of 0.95 or higher, where black, but attempts to keep the emissivity low often resulted in some patches with only a minimal deposit.

Emissivity was measured over an 8 × 8 grid using an R&D Systems AE1 emissometer and was found to have considerable non-uniformity. The emissivity was generally higher than planned but was the best that could be achieved using local suppliers with general purpose plating as

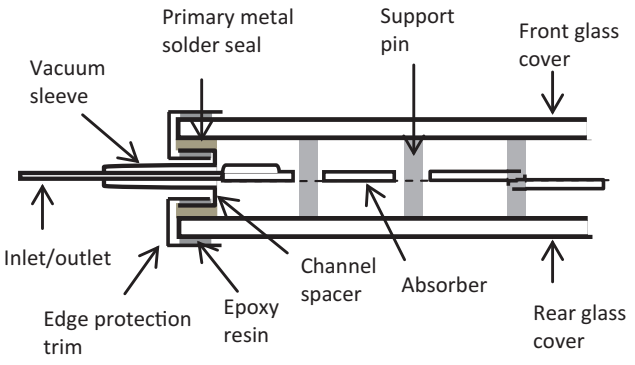

Fig. 1. Collector cross-section (symmetrical enclosure).

Table 1
Design and test parameters.

Aperture area	0.47 m× 0.47 m= 0.221 m^2
Gross area	0.52 m× 0.52 m= 0.27 m^2
Glass thickness	4 mm
Pillar length	25 mm
Pillar diameter	6 mm
Pillar array pitch	60 mm
Absorber through-hole diameter	13 mm
Heat transfer fluid specific heat capacity (J/kg K at 30, 80 °C)	4180–4200 (water + inhibitor)
Typical test flow rate	2 to 6.4 g/s (median 4 g/s)
Typical inlet to outlet fluid temperature rise	−1.8 to +7.4 °C (median 3 °C)

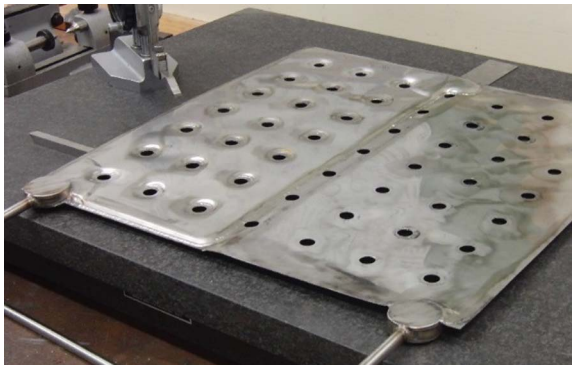

Fig. 2. Absorber prior to black chrome plating.

opposed to specialist solar panel equipment.

3. Test facility and instrumentation

3.1. System components and test procedure

A dedicated solar simulator was designed and built for evacuated panel testing [43], Fig. 3. Four 400 W halogen floodlights provided illumination; the light was directed down through a reflecting box to generate multiple virtual images and achieve uniform illumination without an extensive array of lamps. The illumination level was controlled by a variable transformer. The simulator illumination was calibrated against input power using a Kipp and Zonen CMP-11 pyranometer. The electrical power was measured throughout each test using a Hameg 8115 power meter.

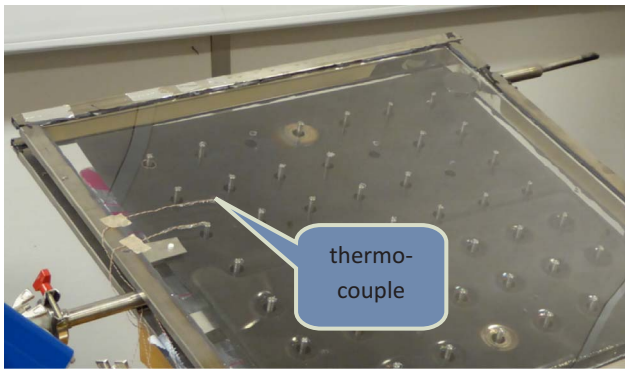

Fig. 4. Enclosure showing top glass thermocouples; the lower glass is instrumented similarly. The support pillars are visible through the glass. The two bare regions result from plating conductors being bolted to these holes.

A circulating bath heated the coolant to the desired test temperature and pumped it up to a header tank from where it flowed under gravity through the absorber and a Coriolis mass flow meter, Fig. 3. Flow temperatures were measured by Pt100 RTDs, two at absorber inlet and two at outlet. Glass temperatures were measured using thermocouples bonded to the glass (Fig. 4) [43].

The vacuum system used an Edwards 18 two stage roughing pump and a Speedivac E04 diffusion pump. Pressures were measured using a KJ Lesker combined vacuum gauge.

Type *T* thermocouples and Pt100 RTDs were used. Thermocouples (Fig. 4) were connected directly to a 16-bit data acquisition system. The RTDs were connected via Weidmuller signal conditioning blocks, with each RTD always using the same block, and were calibrated with cold and hot water in an insulated beaker prior to use. A pair of RTDs was

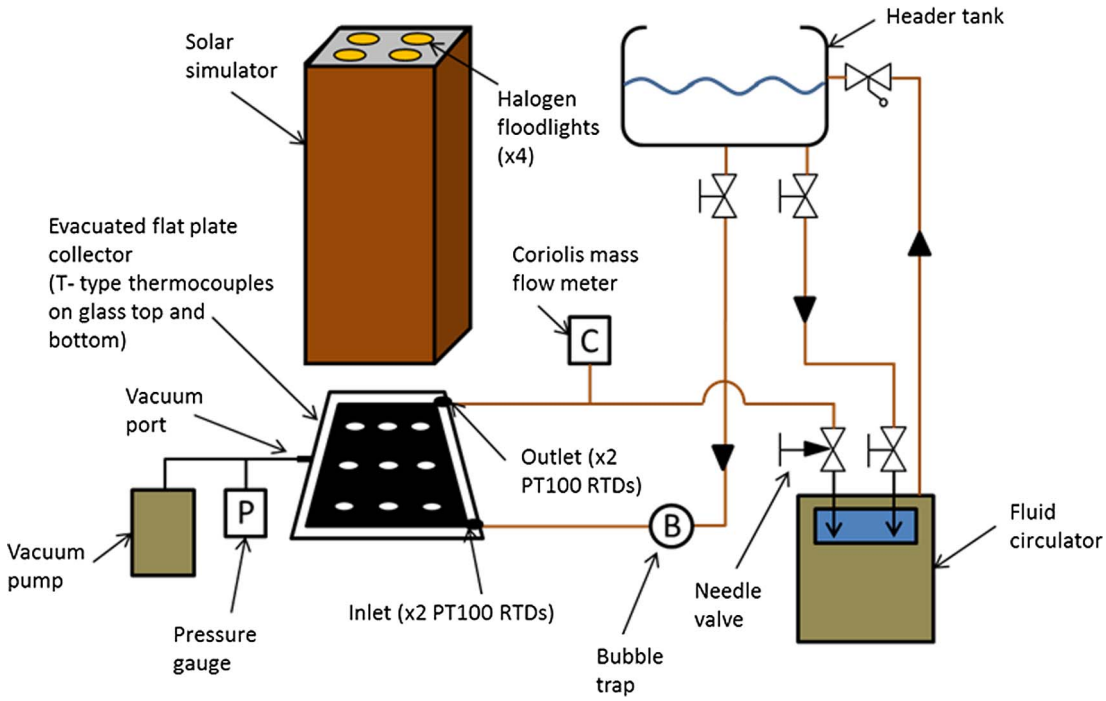

Fig. 3. Schematic diagram of the experimental facility.

used at both inlet and outlet to reduce uncertainty and to check for transducer drift.

During testing the collectors were supported by a 50 mm thick sheet of polyurethane foam insulation to minimise any uncertainty regarding heat losses from the rear.

Once the header temperature was steady, water was allowed to flow under gravity through a bubble trap, the collector, a Coriolis mass flow meter and a needle valve before returning to the bath. The header tank took a considerable time (1–2 h) to reach steady state so testing over the course of a day generally explored a range of illumination levels at a single flow temperature. The absorber time constant was of order 2 min and outlet temperature would largely stabilise about 6 min after changing the illumination. There was however a much slower effect due to the response of the tray and glass.

3.2. Vacuum sealing

The vacuum required continual pumping to maintain a sufficiently low pressure; there was evidence of leakage across the solder seal [7]. This did not affect the accuracy of the experimental measurements but it would clearly be unacceptable for a commercial product. Previous experience in fabricating vacuum glazing samples using indium had successfully achieved a hermetic seal which needed no pump to maintain the vacuum. The main challenge in the development of evacuated flat plate collectors is to achieve sufficient vacuum-tightness that the pressure does not rise above 0.1 Pa over the lifetime of the panel.

3.3. Test stability and instrumentation accuracy

The test data was collected on eight separate days. During each day, the flow temperature was held constant but the illumination level was set to a number of different levels. The flow rate was also adjusted to maintain wherever possible a temperature rise through the absorber in the range 2–8 °C, giving a large enough temperature difference to allow accurate measurement whilst avoiding excessive non-uniformity of absorber temperature between inlet and outlet port areas. The initial time constant of the absorber outlet temperature in response to flow or illumination changes was of order 2 min.

After setting each illumination and flow condition, testing continued until RTD and thermocouple signals appeared sufficiently stable that significantly different values could not be expected were the test to be continued, within a practical time frame. Efficiencies were then calculated as if the data were steady-state i.e. without any correction for transient effects. Stability was assessed by curve fitting the data at each condition to determine the magnitude of the gradient. For the data points in Fig. 5 (below), the stability parameters were:

- mean absolute change in heat flux 0.6% per minute
- mean absolute change in top glass temperature 0.14 °C per minute
- mean absolute change in lower glass temperature 0.08 °C per minute

Coriolis meters are typically accurate to better than 0.1% when measuring liquid flow.

Initial testing showed that the cover glass temperature rose to over 50 °C under the solar simulator. Subsequent investigation [43] showed there to be a long wavelength (> 3000 nm) infra-red component of the floodlight spectrum which is absorbed by the glass instead of passing through. Simulations suggested that the efficiency with this illumination spectrum is approximately 1% higher than the efficiency under a nominal AM1.5 solar spectrum, if the efficiency is based on the pyranometer power reading and there is no change in cover glass temperature. A fan blowing over the top surface was used to limit the glass temperature.

4. Test results

Test results under both atmospheric and high vacuum conditions are shown in Fig. 5.

The fact that the vacuum and non-vacuum tests each lie close to a best-fit straight line indicates that U_L did not change significantly over the testing range of fluid temperatures, T_M = 20,31 and 51 °C.

These U_L mean heat loss coefficients are higher than commercial standards because of the poor emissivity of the black chrome plating. The difference between the 1 bar and evacuated U_L values, 3.7 W/m^2 K, demonstrates the reduction in heat losses possible in an evacuated system.

A steady-state heat balance simulation (Fig. 6, Table 2) investigated the necessary parameters for matching experimental data from the solar simulator. The algorithm takes a pair of absorber and environment temperatures and solves a quartic heat balance equation to determine the upper and lower cover glass temperatures:

$$-(\varepsilon_{pg,i}+\varepsilon_{eg,i})\sigma T_{g,i}^4-(h_{i,i}+h_{o,i})T_g+(\varepsilon_{pg,i}T_p^4+\varepsilon_{eg,i}T_{env}^4)\sigma+h_{i,i}T_p+h_{o,i}T_a+q_{abs}=0,\quad i=1{,}2\ \text{(upper,lower)}$$

Heat transfer within the enclosure was predicted using radiative and low-pressure conduction models; external heat transfer used a given heat transfer coefficient to model the effect of the cooling fan (top) and the insulating support pad (underneath). The glass emissivity was taken as 0.96.

To match the measured efficiency and upper glass temperature the absorber top surface emissivity was raised above the measured levels.

An IR component equivalent to an additional 14.5% of the incident power [43] is included in the model and contributes to heating the upper glass cover. The fan increases the upper surface heat transfer coefficient above the 5.6 W/m^2 K expected by natural convection. The increase in lower surface heat transfer coefficient mimics the transient effect of the lower glass being cooler than expected. The best fit combination of emissivities and heat transfer coefficients is dependent on the assumption that the thermocouples properly determine the mean glass surface temperature. This is unproven: some deviation from the expected values is unsurprising.

The general trend of efficiency in Fig. 6 following the experimental points suggests that the necessary physical phenomena are being correctly modelled and that the simulation code may safely be used to predict performance for an optimised panel with a lower emissivity coating.

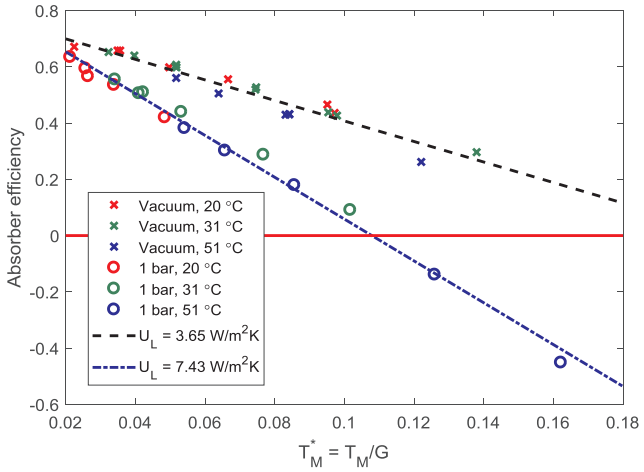

Fig. 5. Efficiency test results for atmospheric and high vacuum tests. The vacuum pressure was less than 0.03 Pa. 95% confidence limits for U_L: [3.52, 3.78] and [7.02, 7.85] based on line fit statistics.

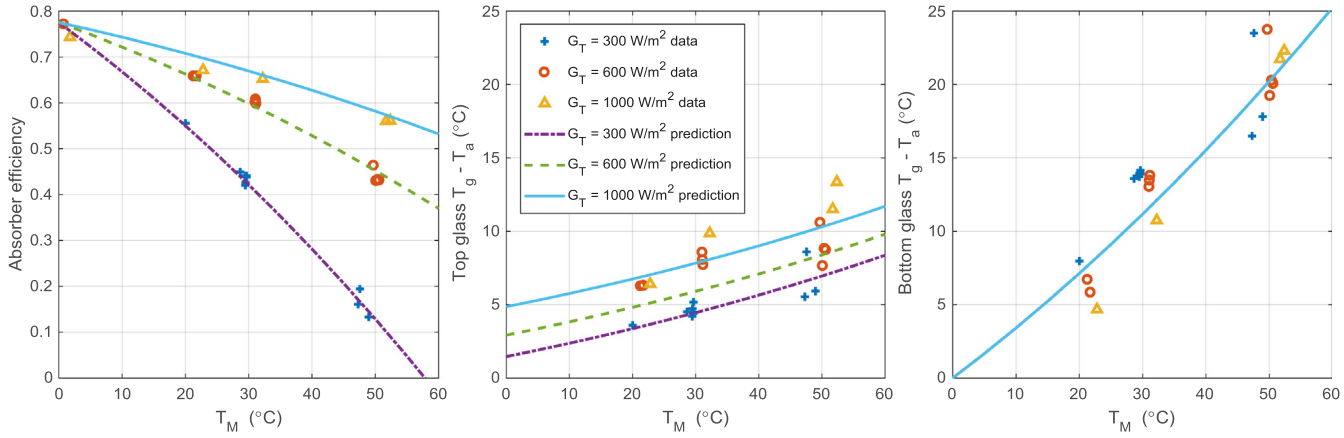

Fig. 6. Comparison of data with simulations (evacuated, fan on).

Table 2
Comparison of estimated emissivities with best fit values.

	Experiment	Simulation
Upper surface h (W/m^2 K)	Unknown	22
Absorber top α,ε	Unknown, 0.385	0.82, 0.46
Absorber underneath ε	0.15	0.15
Lower surface h (W/m^2 K)	0.44	1.8

5. Simulations of performance based on weather data

5.1. Comparison with alternative solar collectors and PVT panels under constant conditions

Fig. 7(a) compares a simulation of an optimised evacuated flat plate against typical efficiency trends for each kind of solar collector. The optimised simulation included anti-reflection coatings on both sides of the top cover and a selective absorber coating with $\alpha = 0.96$, $\varepsilon = 0.04$; coatings of this standard are commercially available. The simulation described in Section 4 above was adapted to model outdoor applications by including terms for radiation to the sky and convective heat transfer from the top cover. Mean relative humidity (72%) and daytime wind speed were obtained from six years' data from the University of Warwick weather station, located on top of the School of Engineering building in Coventry at 52°22′56″N, 1°33′43.5″W, [44]. Coventry was taken as having a typically temperate European climate.

The mean convective heat transfer coefficient, 5.2 W/m^2 K, was calculated from $h_w = \frac{8.6V^{0.6}}{L^{0.4}}$ [70] and assumes a characteristic building dimension of 8 m (after Duffie and Beckman). 5.2 W/m^2 K is equivalent to a weighted mean wind speed of 1.73 m/s from the weather data. To facilitate comparisons between flat plate and tubular collectors the efficiencies in Fig. 7 have been based on gross area: $\eta_g = \frac{A_A}{A_g}\eta_A$.

The collectors in Fig. 7 were chosen for comparison purposes as examples of the higher efficiency models in the SPF online catalogue (Table 3). Their test data was downloaded from DIN CERTCO and correlated in terms of a cubic heat loss model:

$$\eta_g = \eta_0 - \frac{\alpha_1 T_M + \alpha_2 T_M^2 + \alpha_3 T_M^3}{G}. \quad (1)$$

To further validate the collector efficiency model described in Section 4, a simulation was performed to match the DIN CERTCO data points for the TVP evacuated panel. The parameters listed in Table 4 were found to closely model the TVP test result and are within the expected range for coating absorbance and emissivity.

The experimental absorbers and optimised simulation have in theory a slight advantage in that the flooded panel configuration achieves a collector efficiency factor $F' = 0.998$ as opposed to an estimated 0.968 for the tube-on-plate TVP design.

The experimental heat loss coefficient for the high vacuum fitted line in Fig. 5 (referred to gross area; absorber area values are 17% higher) is approximately 3 W/m^2 K at $T_M = 50$ °C. The optimised simulation shows this could be reduced to 0.42 W/m^2 K by using a high quality coating.

The published performance of the TVP panel comes close to the

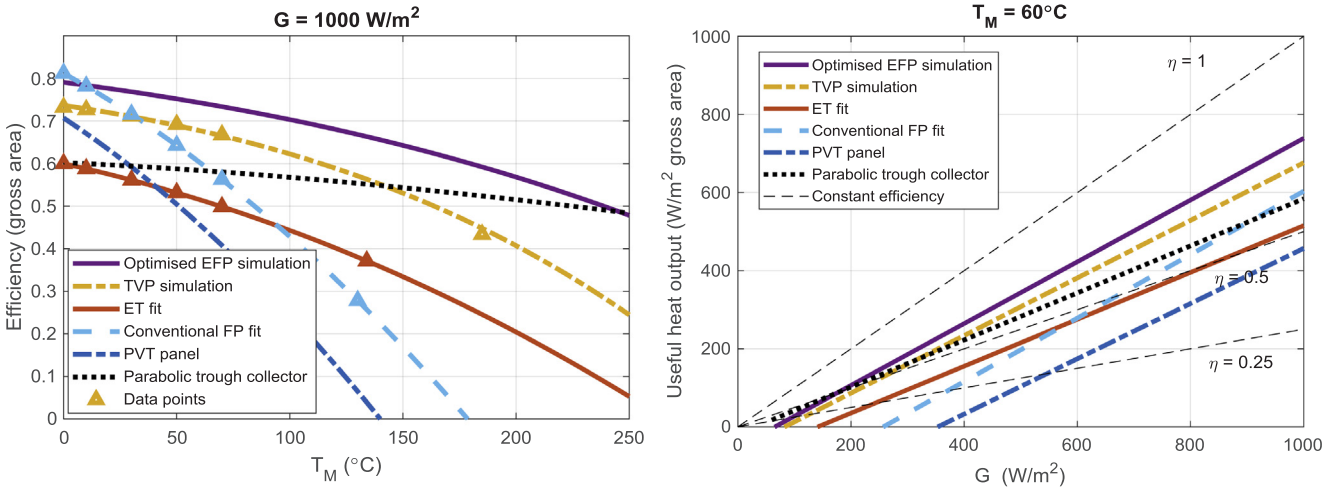

Fig. 7. (a) Comparison of different collector technologies at $G = 1000$ W/m^2. (b) Predicted output as a function of insolation (G) at $T_M = 60$ °C.

Table 3
Data sources used for Fig. 7.

Key	Type	Manufacturer	Model	Data source
Optimised EFP	Evacuated flat plate	Simulation only		
TVP simulation	Evacuated flat plate	TVP	V3 KeyMark test	[69] website
ET	Evacuated tubes	EnerTec	Enersol HP 70–24	[69] website
Conventional FP	Flat plate	Savo-Solar	SF500-15	[69] website
PVT	Combined PV/Thermal panel	Simulation [45] with maximum electrical output		
Parabolic trough collector	Concentrating collector	NEP Solar	[46]	Web site (NEP simulation)

Table 4
Evacuated flat plate simulation parameters used for Fig. 7.

	TVP collector	Optimised collector
Glass transmittance	0.948	0.97
Coating absorbance	0.87	0.95
Coating emissivity	0.07	0.04
Collector efficiency factor F'	0.968	0.998
External heat transfer coefficient (W/m^2 K)	5.2	5.2
Thermal bridging loss ($\Delta\eta$ at T_M = 50 °C)	0.02	0.02
Aperture: gross area ratio A_A/A_G	0.849	0.86

optimised design simulated here. At $G = 1000\ W/m^2$ the optimised evacuated panel has higher efficiency than other designs up to $T_M = 245$ °C: beyond this point the parabolic trough collector is more efficient, albeit only in clear conditions when beam radiation is available.

At this high radiation level and $T_M = 60$ °C an optimised evacuated flat plate could collect 13% more heat than a conventional flat panel or 32% more than the same area of evacuated tubes; this increases to approximately 50% relative to either flat panel or evacuated tube at $T_M = 100$ °C.The PVT panel in Fig. 7 is a simulation described as "state of the art" by Matuska et al. [45] that predicted the performance that should be possible from a single-glazed flat panel collector with PV cells bonded to the absorber surface. The thermal efficiency is lower than a comparable flat plate collector due to the electrical power extraction: the curve represents operation with maximum electrical output.

The parabolic trough collector in Fig. 7 (PolyTrough 1800) [46] has a concentration factor of 54. Its efficiency curve was taken from the manufacturer's data sheet as a DIN CERTCO certificate was unavailable. The gross area in Fig. 7 was estimated for vertical illumination, assuming the closest trough pitch (2 m) allowing full rotation without interference. Trough arrays are generally arranged in a horizontal plane whereas flat plate and evacuated tube collectors are usually mounted on a sloping roof. At lower incidence angles the PTC fill factor increases slightly, improving the efficiency and moving the intercept with the EFP curve down to $T_M = 210$ °C.

Domestic hot water applications do not require this high temperature capability but can benefit from the reduced heat loss at low irradiance levels. Useful heat output is commonly defined as $Q_u = G(\tau\alpha) - U_L T_M$ [70]. At constant T_M the heat loss coefficient U_L is expected to be constant. This results in a linear relationship between irradiance G and output Q_u, Fig. 7(b). For $T_M = 60$ °C the heat output from the conventional panel becomes negative below a critical radiation level $G = 250\ W/m^2$ i.e. the circulating pump would need to be switched off to prevent the water cooling down. The evacuated flat panel reduces this critical level to $60\ W/m^2$.

5.2. Simulation of monthly heat output, at constant delivery temperature, using historical weather data

A number of researchers have studied the transient response of solar collectors or used weather data as a basis for comparisons. Zambolin and Col [47] compared flat plate and evacuated tubes collectors, obtaining daily average efficiencies. Zima and Dziewa [48] measured and modelled the fluid outlet temperature from a flat plate collector. Rodríguez-Hidalgo et al. [49] studied the importance of thermal inertia in collector efficiency models. Amrizal et al. [50] measured the time constant for fluid outlet temperature from a PVT panel following a radiation step. Gao et al. [51] simulated evacuated tube transient response for water-filled and U-tube collectors and found that heat capacity effects required modelling to avoid over-prediction of the heat output. Agrawal and Tiwari [52] used average hourly climate data at four locations in India to predict performance for a PVT module.

The University of Warwick weather data includes irradiance, wind speed and temperature sampled at 1 min intervals over six years (2011–2017). The distribution of irradiance G for all times when the Sun is above the horizon and in front of a south-facing panel at 30° to the horizontal is shown in Fig. 8. As an indication of the local climate, the "Clear sky" line shows the predicted irradiance distribution (due to solar angle to panel and zenith angle) if every day were clear. The air temperature over the same period is very close to a Normal distribution with mean 13.2° and standard deviation 5.9 °C.

The weather data set was used in a simulation of collector heat outputs for four different styles of collector, Fig. 9(a).

The University of Warwick district heating main was taken as a notional example of a vacuum insulated collector application. The pyranometer recorded the total (beam plus diffuse) radiation levels: an algorithm (Appendix A) was used to estimate the beam component and include incidence angle modifier effects.

The simulation uses a transient response algorithm which imports the data set for each month and predicts the absorber temperature and heat output for each minute using a time-marching scheme (Appendix B). In terms of functionality it is similar to ScenoCalc [53] which is used by SPF to generate DIN CERTCO certificates. Whereas ScenoCalc is an Excel application however, the present code uses Matlab to simplify importing over 3 million weather data records and generating outputs spanning a wide range of absorber temperatures.

The algorithm assumes that the heat transfer fluid would be pumped whenever the net heat output was positive and turned off at other times; when pumped, the fluid would be limited to the heating main

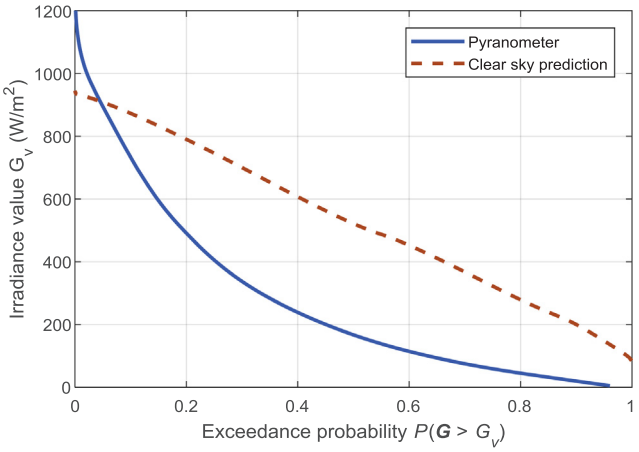

Fig. 8. Annual irradiance distribution from University of Warwick weather data.

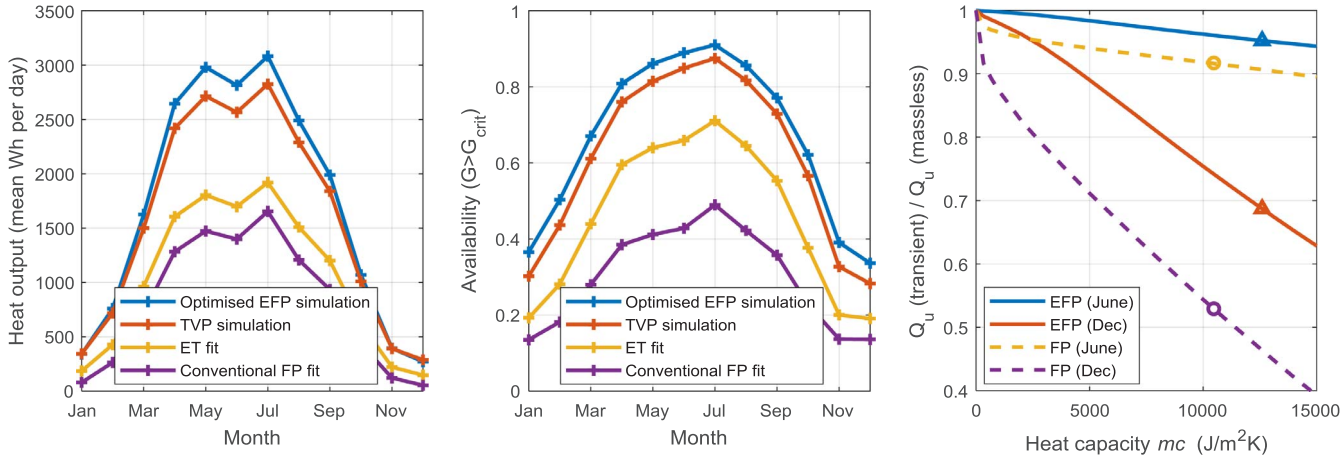

Fig. 9. (a) Predicted heat transfer to a district heating main based on weather station insolation and ambient temperature data for 2011–2017, assuming that the pump switches off whenever the heat flux would be negative. (b) "Availability" when insolation exceeds the critical level. (c) Effect of varying the absorber heat capacity for the optimised collector and conventional flat panel. Data points show nominal *mc* values. See Table 3 for abbreviations.

temperature (taken for simplicity as a constant, T_{HM} = 85 °C). While G is below the critical level (whether over-night or during a period of poor light) the model predicts absorber temperature to determine when the next heat delivery period begins.

Fig. 9(b) shows the annual variation in "availability", defined as the fraction of the time with sun shining on the collector for which the insolation exceeds the critical level at the heating main temperature.

Comparison of the transient temperature analysis with one based purely on the instantaneous radiation level shows the impact of absorber heat capacity on monthly output, Fig. 9(c).

In June the weather is warm and relatively little time is lost while raising a cold absorber up to the heating main temperature; conversely in December transient effects become more significant. The dependence on heat capacity *C* seen in Fig. 9(c) shows that in Winter the absorber is regularly cooled towards an asymptotic level (ambient) as opposed to following a short-term linear cooling and heating time history. The latter case would not be significantly influenced by varying a panel's heat capacity. The heat capacities used for Fig. 9(a) and the associated annual efficiency and heat output are given in Table 5.

5.3. Panel area required to meet a low-temperature heat demand in Winter

UK is committed to cutting its carbon dioxide emissions by 2050 to 20% of the 1990 level. It may be very difficult to substantially reduce emissions in some industrial and transport applications. Domestic heat and hot water supplies may therefore have to be almost completely carbon-neutral by that date.

One option would be to install a sufficient area of evacuated solar collectors to supply the required heat, even in cold weather with low radiation levels. Conversely a PV or PVT panel could be used with the electrical output driving a heat pump. The PV panel has a potential advantage in that it can be located at a distance from the property and even perhaps in a country with more sunlight in Winter.

A "PHRIE 95" air source heat pump [54] was empirically modelled as:

$$COP = 0.578 COP_{Carnot} - 1.29, \quad 1 \leqslant COP \leqslant 5$$

The Carnot cycle COP was based on absorber temperature and air temperature from the weather data.

Fig. 10 compares the output predicted using the December weather data for an evacuated flat plate, conventional evacuated tubes and flat plates, Matuska's PVT and a PV panel; any electrical output is converted to heat via a heat pump. PV and PVT electrical efficiency was assumed [45] to be

$$\eta_e = 0.15 e^{-0.0045(T - 25\,^\circ\mathrm{C})} \quad (2)$$

The cross-over point at 58 °C shows that above this temperature the panel area required to meet the heat demand would be smaller for the evacuated flat plate. The heat pump COP increases as the delivery temperature is reduced and below 58 °C a PVT panel plus heat pump could meet the demand with a smaller area than evacuated flat plates. Either option would require thermal storage to provide heat on demand throughout the day.

Given sufficient storage a temperature of 40 °C would be sufficient for domestic hot water. The graph shows a clear advantage in adopting under-floor heating and similar means for using heat at the lowest possible temperature to minimise the required panel area.

At 40 °C the PV + HP curve in Fig. 10 requires 37% more area than the PVT + HP. A map of daily mean solar radiation over Europe in December [55] shows approximately 0.45 kWh/m^2 over Coventry compared with 2.2 kWh/m^2 in southern Spain. Given a sufficient electrical transmission capability with a nominal 90% efficiency it might be possible to replace 1 m^2 of roof-mounted PVT panel in the UK with 0.31 m^2 of PV panel in Spain, to generate the same heat output at 40 °C in December.

5.4. Annual output from thermal and PVT panels as a function of delivery temperature

A number of papers have described possible combined heat and power (CHP) applications for high efficiency solar collectors using either hybrid PVT panels or (Section 5.5) thermal panels driving Stirling engines or Organic Rankine Cycle (ORC) systems.

Ancona et al. [56] investigated the suitability of a dish array to illuminate a high efficiency PVT collector. Crisostomo et al. [57] studied the use of selectively absorbing nanofluids in PVT collectors. Modjinou et al. [58] tested a novel PVT panel based on micro-channel heat pipes.

Table 5
Estimates for absorber heat capacity used for the Fig. 9 (a, b) simulations together with mean annual output (kWh/m^2 gross area) and annual mean efficiency over the weather data illuminated period for an absorber temperature of 85 °C.

	Heat capacity *C* (J/m^2 K)	Annual output (kWh/m^2)	$\bar{\eta}_{85\,^\circ\mathrm{C}}$
Optimised evacuated flat plate	12,600	678	0.607
TVP	5300	594	0.532
Evacuated tube	4700	392	0.351
Flat plate (Savo SF500 microchannel)	10,500	333	0.298

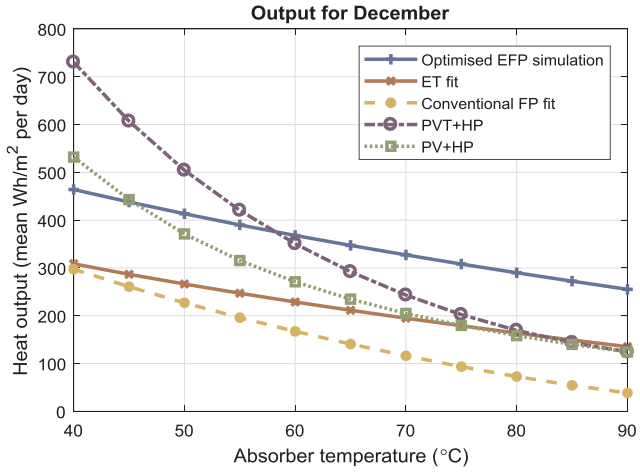

Fig. 10. Potential to deliver DSHW heat in December as a function of delivery temperature.

Bianchini et al. [59] compared the performance and installation costs of PVT panels against separate PV and solar thermal collectors and concluded that a conventional flat plate collector performed better in Winter than his PVT collector due to the latter's high loss coefficient, $U_L = 14.4$ W/m^2 K.

Compared with a PVT panel, an evacuated flat plate has a much lower heat loss coefficient U_L and is likely to produce more heat in cold conditions with weak insolation; conversely in terms of energy pricing electricity is more valuable than heat. A cost-benefit analysis was performed assuming $v = \frac{\text{Cost of electricity (£ / kWh)}}{\text{Cost of gas (£ / kWh)}} = 3.2$ (as Moss [36]) leading to a definition of instantaneous Equivalent Thermal Output $Q_{eq,Th} = Q_{th} + vW_{elec}$ (Watts) and annual total output for a PVT (or thermal panel, setting $W_{elec} = 0$):

$$E_{eq,Th} = \int_{1\ \text{year}} (Q_{th}^{+} + vW_{elec})\mathrm{d}t \quad \left(\text{Wh/m}^2\right)$$

This provides a clearer insight into the merits of each system than an exergy analysis. If the installation used the electrical output of the PVT panel to power a heat pump with a coefficient of performance $COP = 3.2$ the total heat output would equal $E_{eq,Th}$. Heat pumps typically provide a COP in this range at delivery temperatures of 35 °C but COP falls at higher temperatures.

A similar analysis to Section 5.2 investigated the dependence of E_1 on evacuated flat plate absorber temperature over the six year weather data period, Fig. 11.

When comparing flat plate efficiencies with the PTC beam power efficiency at $G_T = 1000$ W/m^2 (Fig. 7(a)) it should be noted that the beam component estimated from the weather station data is only 52% of the total radiation (2.10 GJ/m^2 versus 4.02 GJ/m^2 annually). Parabolic trough collectors typically capture none of the diffuse radiation component: they therefore perform poorly in comparison to the evacuated flat plate at the lower temperature limit in Fig. 11. The weather data simulation used a trough pitch of 2.13 m which for a latitude of 52° results in zero shading and highest fill factor at the maximum solar elevation (60°). For comparison purposes, gross area for a trough array is defined here as the projection of the horizontal trough array area onto a 30° slope. The intention was for the projected beam-normal area to match the slope-mounted FP, ET and PVT collector areas when the Sun was due South at 60° elevation. The trough collectors were assumed to track in elevation about an East-West axis but not in azimuth.

At the lowest temperature in Fig. 11 (60 °C) the value of energy produced annually by a PVT panel (dashed line) is 59% higher than for a conventional flat plate and 4% higher than for the optimised EFP. This matches the conclusions of Herrando and Markides [60] regarding the potential benefit in terms of CO_2 emissions from using PVT panels in a domestic context. Above 70 °C however the EFP becomes the most profitable, producing for instance 56% more energy value at 130 °C than the PVT panel.

A hybrid PVT panel could in principle be evacuated to improve the high temperature efficiency: this would give a higher equivalent thermal output than any of the cases simulated here. Such a panel would require PV cells and wiring with very low outgassing rates. This has yet to be realised for flat plate PVT collectors; Abdelhamid however [61] tested a concentrating PVT collector with vacuum-insulated GaAs cells cooled by mini-channels, achieving 8% electrical efficiency together with 33% thermal efficiency at 365 °C.

The parabolic curve fits in Fig. 11 characterise the annual thermal output for analytical purposes as

$$E_1 = \int_{1\ \text{year}} Q_1^{+}\mathrm{d}t \approx aT_{1K}^2 + bT_{1K} + c \quad \left(\text{Wh/m}^2\right) \tag{3}$$

The coefficients in Table 6 are defined in terms of absolute temperature T_{1K} for compatibility with Section 5.5.

5.5. Potential applications in conjunction with an organic Rankine cycle

5.5.1. Effect of varying cycle peak temperature T_1

The thermal output from a solar collector at absolute temperature T_1 may be used to drive a heat engine that rejects heat at temperature T_2. This can be an effective way of either (i) generating power in situations where the rejected heat has no value or (ii) generating a more modest power output when the primary purpose is heat generation (for water, space heating or storage) but the solar collector is able to operate efficiently at a higher temperature than the application requires. A thermal system sized to provide a useful thermal output in Winter is likely to produce a surplus of heat in Summer: this surplus heat can drive an ORC to generate electricity.

Concentrating solar generating stations [17] operate in the first mode and are in competition with photovoltaic (PV) panels. These are typically large installations using concentrating collectors and a steam Rankine cycle; they operate in venues with very little cloud cover.

The second situation might use non-concentrating collectors to generate heat even in conditions of diffuse light. Temperatures are generally lower than with concentrating collectors leading to the use of organic fluids instead of water for the power cycle. Freeman et al. [13] investigated solar thermal collectors supplying heat to an Organic Rankine Cycle (ORC) and Lee et al. [62] used a solar chimney to power an ORC. Quoilin et al. [63] studied the optimal design of a trough collector coupled to an ORC. None of these papers evaluated the performance of an ORC relative to the PV or PVT alternative.

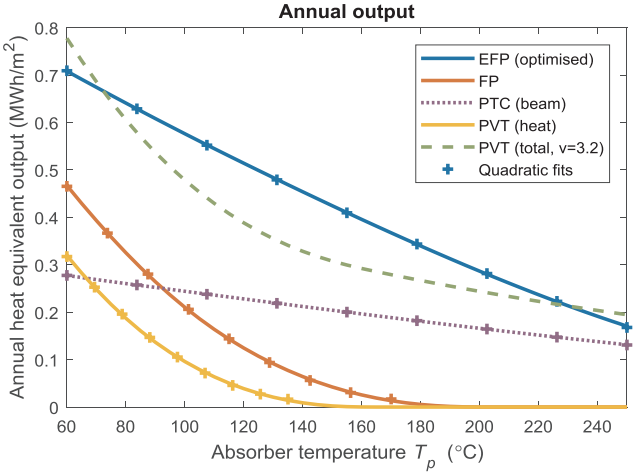

Fig. 11. Effect of absorber temperature on annual heat output and (PVT) combined equivalent output $E_{eq,th}$.

Table 6
Curve fit coefficients for Fig. 11 ($60 \le T_p \le 250$ °C, $E_1 > 0.01$ MWh/m^2).

	A	B	c
EFP (optimised)	3.204×10^{-6}	−0.005592	2.216
FP	3.217×10^{-5}	−0.02905	6.572
PTC (heat)	4.475×10^{-7}	−0.001155	0.6127
PVT	4.379×10^{-5}	−0.03647	7.607

The excellent medium-temperature efficiency of an evacuated flat plate collector suggests that it might find some application as an ORC or Stirling engine heat source in place of concentrating collector designs and that this combination might challenge PVT collectors in providing both power and heat. A simple simulation has been performed to test this hypothesis: as above, the concept of a "equivalent thermal output" with cost ratio $v = 3.2$ has been used to provide a single performance metric. The electrical efficiency of an organic Rankine cycle may be defined as a "Second Law efficiency" (fraction of the Carnot cycle efficiency) between the same temperatures, $f = \frac{\eta_{ORC}}{\eta_{Carnot}}$. The efficiency ratio f typically lies in the range 0.3–0.5 [64,65] and depends on choice of working fluid together with the alternator and expander efficiencies; the highest value identified by Landelle was $f = 0.6$.

The equivalent instantaneous thermal output may be defined in terms of source and sink absolute temperatures T_1,T_2 and the heat flux Q_1 obtained with the absorber at T_1:

$$Q_{eq,Th} = Q_1(1-\eta_{ORC}) + vQ_1\eta_{ORC}$$
$$= Q_1\left(1 + \left(v-1\right)f\left(1-\tfrac{T_2}{T_1}\right)\right) \quad \left(\mathrm{W/m^2}\right)$$

To allow a significant cycle efficiency at modest source temperatures the sink temperature T_2 was set at 333 K (≈ 60 °C) as opposed to the 85 °C heating main temperature in Section 5.2. 60 °C would be sufficient for domestic hot water or a lower temperature "Fourth Generation" heating main.

It was assumed that any practical ORC would operate between two fixed temperatures dictated by the choice of organic fluid and that its output power could be modulated depending on the heat input. The model assumed for simplicity that sufficient flow of heat transfer fluid could be provided such that any temperature differences between absorber and ORC maximum, or ORC minimum and hot water sink, would be small enough to be neglected.

The annual energy output is a function of the time history of the heat flux from the collector operating at temperature T_1:

$$E_{eq,Th} = \left(1 + \left(v-1\right)f\left(1-\frac{T_2}{T_1}\right)\right)E_1 \quad \left(\mathrm{Wh/m^2}\right) \tag{4}$$

Fig. 12 compares the equivalent thermal outputs from Matuska's optimised PVT panel and a range of ORC systems using the optimised evacuated flat plate (EFP), a conventional flat plate (FP) and a parabolic trough collector (PTC) as heat sources. The four lines for each collector show the output from imaginary ORC cycles with 0, 33%, 67% or 100% of the Carnot cycle efficiency. Even if the thermal collectors were coupled to a heat engine achieving the Carnot efficiency, the combined output would still be less than from the PVT panel.

It may be concluded that thermal collectors are advantageous for installations where PVT panels could not provide sufficient heat or applications where the temperature exceeds PVT limits; conversely PVT panels can provide a higher revenue stream in terms of the value of energy produced.

Fig. 12 shows that at a given peak temperature T_1 the addition of an ORC increases the equivalent thermal output, provided that the heat is required at some lower temperature T_2. There is however a second effect that is usually more significant, namely that reducing T_1 increases the thermal output of the collector. For typical values of f,v and $\frac{U_L}{G}$ the highest equivalent output might in practice be achieved at $T_1 = T_2$, in which case the ORC output power is zero and it serves no purpose. This assumes that the full heat output can be utilised; if not, the electrical output is of value regardless of any associated drop in heat output.

5.5.2. Identification of optimum peak temperature T_1 for an Organic Rankine cycle

By differentiating Eq. (4) it can be shown that with a given ORC heat rejection temperature T_2 the peak equivalent thermal output occurs at an optimum absorber temperature $T_{1,opt}$ that satisfies the cubic equation

$$2a(1+\mu)T_{1,opt}^3 + (b(1+\mu) - \mu a T_2)T_{1,opt}^2 + c\mu T_2 = 0$$
$$\text{where } \mu = (v-1)f. \tag{5}$$

If Eq. (3) is replaced by a linear fit $E_1 = bT_1 + c$, i.e. setting $a = 0$, Eq. (5) has an explicit solution $T_{1,opt} = \sqrt{\frac{-\mu c T_2}{(1+\mu)b}}$.

These optimum temperature points have been used to identify the curve maxima in Fig. 12. Selecting a lower heat rejection temperature T_2 would raise the work output but in practice T_2 will be constrained by the intended application (space heating, hot water, thermal storage) for the heat from the ORC.

If the heat cannot be used in Summer the best T_2 would be the lowest temperature available for heat rejection from the ORC. The heat could for instance be delivered to a bore hole to balance heat extraction in Winter. Defining the electrical output as $W_{elec} = \eta_{ORC}E_1 = f\left(1-\frac{T_2}{T_1}\right)(aT_1^2 + bT_1 + c)$, the highest electrical output for a given collector area would be achieved when $T_{1,opt}$ satisfies $2aT_{1,opt}^3 + (b - aT_2)T_{1,opt}^2 + cT_2 = 0$.

5.5.3. Optimal choice of PVT, EFP + ORC or EFP + PV at constant thermal output

The simulation for Fig. 12 investigated annual heat delivery via an Organic Rankine Cycle with sink temperature 60 °C. Lower temperatures are also of interest, particularly in conjunction with thermal storage systems. A thermal storage system requires an annual heat input to balance the heat extracted plus losses: it might in theory also generate a power output, if a sufficiently efficient thermal collector and ORC combination were available. This section investigates whether there are any circumstances in which an ORC combination could challenge the simplicity of either a PVT array or an EFP + PV system with the same area of panels.

Borehole thermal energy storage [66] typically uses solar collector heat in Summer to raise temperatures underground. Chapuis and

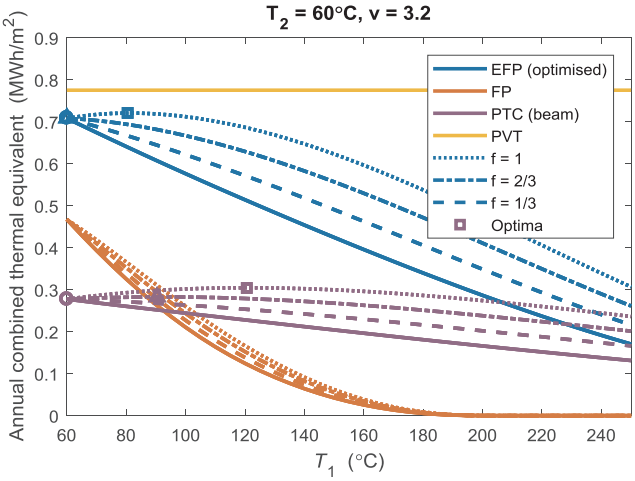

Fig. 12. Annual combined thermal and electrical output, expressed in terms of thermal energy values, for systems delivering heat at 60 °C. Solid lines are the collector heat output at absorber temperature T_1, equivalent to $f = 0$.

Bernier [67] studied a Canadian district heating system. They simulated two systems with different ratios of storage volume to collector area, resulting in borehole temperatures that cycled between 45 and 70 °C (9.6 m^3 storage per m^2 collector) or, for lower heat losses, 10 and 15 °C (154 m^3 storage per m^2 collector). The latter option in conjunction with a heat pump achieved much lower heat losses as well as improved collector efficiency.

Ground temperatures at 1 m depth in the UK range from 8.8 to 12.7 °C (North-South) and rise by 2.6 °C per 100 m depth increase [68]. As a conservative estimate for the present investigation it was assumed that an ORC rejecting heat to a borehole might operate with heat rejection at 25 °C and be used to produce power for the six months April–September while charging the heat store. The highest feasible efficiency ratio $f = 0.6$ was assumed for the ORC. Fig. 13 compares the possible electrical output from an ORC against the same area of PV panels. The annual thermal output profile from Fig. 11 results in a peak electrical output for an EFP-heated system when the peak temperature is 142 °C, Fig. 13. A similar system heated using a parabolic trough collector would generate peak power at 191 °C but the inability to utilise the diffuse radiation component present in the Coventry weather data results in the PTC electrical output being only half the EFP equivalent.

At $G < 1000$ W/m^2 the efficiency curves in Fig. 7(a) compress towards the y-axis in accordance with Eq. (1). At 400 W/m^2 (upper quartile of G, Fig. 8) the EFP and PTC efficiency curves would intersect at $T_M = 125$ °C. i.e. $\eta_{PTC} > \eta_{EFP}$ for $T_M/G > 0.31$. If the PTC were replaced by a hypothetical collector having the PTC efficiency curve but the EFP's ability to absorb diffuse radiation, the peak output ("PTC (all radiation)" curve, Fig. 13) would increase by 117%. The differences between curves in Fig. 13 illustrate the effects of lowering U_L (EFP versus PTC all radiation) and then losing the diffuse component (PTC beam only). For reference, increasing the beam fraction to 82% (clear day), with the same irradiance, would raise the "PTC beam only" output by a mere 47% because of the area sensitivity to incidence for beam radiation.

The university has an array of PV panels near the weather station: rather than using the electrical output data, however, a simulated output was derived from the same pyranometer values used in the thermal collector predictions to ensure strict comparability. PV efficiency falls with panel temperature: the temperature of PV panels adjacent to the weather station was correlated as $T_{panel} = T_a + \frac{G}{28.36 + 5.86V}$ (residual error 2.1 °C rms) and used in Eq. (2) to predict efficiency. Monthly mean PV output was then predicted from the weather station data. The mean PV efficiency in Fig. 13 is 14.6% corresponding to an effective mean panel temperature of 31.6 °C.

The electrical output per m^2 for the EFP collector plus ORC in Fig. 13 is 51% of the PV panel output (59% for PTC "all radiation"); conversely the PV panel produces no useful heat. A PVT panel would have similar electrical efficiency to the PV panel but (currently) lower thermal efficiency than an EFP collector.

The EFP with an absorber temperature of 25 °C delivers 623 kWh/m^2 heat over April–September. Any system generating electricity in addition to heat will require a larger collector area than one sized purely for the thermal output. Fig. 14 shows the electrical output from a larger collector area for four systems designed to deliver 623 kWh heat over 6 months to a 25 °C thermal store i.e. equivalent in thermal terms to an EFP of 1 m^2. The options considered were:

- EFP + ORC ($f = 0.6$)
- PTC + ORC ($f = 0.6$), beam only
- PTC + ORC ($f = 0.6$), all radiation
- EFP (1 m^2) + PV (remainder)
- PVT (1.23 m^2) + PV (remainder).

The EFP/ORC maximum efficiency point at 2.1 m^2 is very close to the EFP + PV line in Fig. 14: this is coincidental. The combination of a PVT panel to provide the required heat output plus additional PV panels to cover any available area provides the highest electrical output of these three options. Whilst the EFP plus ORC combination can provide more electricity than EFP + PV for panel area ratios up to 2.1, this is not a sensible option given the complexity of such a system and the superior output from a PVT + PV combination. The PTC + "beam only" ORC output is significantly less than the EFP equivalent and even the hypothetical "all radiation" case cannot match the PVT performance.

A fifth possibility would be to use a larger area of PVT panels instead of PVT + PV: this would give the same electrical output while increasing the heat output.

5.5.4. Efficiency requirements for thermal power cycles to compete with PV panels

The poor electrical efficiency of the organic Rankine cycles relative to the PV panels described above stems from the inevitable thermodynamic limitations of a heat engine cycle coupled with falling collector efficiency at high temperatures and low irradiance. Given selective coatings significantly better than the current state of the art and/or a sufficiently high concentration ratio it might however be possible for solar thermal power cycles to match PV efficiency levels.

Defining the electrical efficiency of a heat engine cycle (whether ORC, steam Rankine or Stirling engine, driving an alternator) as $\eta_{Elec} = f\eta_{Carnot}\eta_G = f\left(1-\frac{T_2}{T_1}\right)\eta_G$ the necessary collector gross efficiency η_G at an absorber temperature T_1 to match a PV panel efficiency η_{PV} is given by $\eta_G = \frac{\eta_{PV}}{f\left(1-\frac{T_2}{T_1}\right)}$.

The predicted annual heat output (Fig. 11) may be characterised in terms of the annual insolation on the pyranometer plane and a mean efficiency at each absorber temperature:

$$E_1 = \bar{\eta} \int_{1\ \text{year}} G\,dt$$

Fig. 15 compares these weather-data based mean efficiencies with the collector efficiency required (blue line) to enable an ORC operating at $T_2 = 25$ ° C= 298 K, $f = 0.6$ to match a 15% efficient PV panel.

Under constant G = 1000 W/m^2 beam irradiance and working at the optimum temperature, the efficiency curves for EFP + ORC and PTC + ORC each come within 9% of the target (blue line) to match a PV panel. Under Coventry weather conditions however (taking the 12 monthly output, Fig. 11) the mean irradiance is lower, leading to reduced efficiency at each temperature point. The curves based on the entire pyranometer irradiance (EFP, PTC "all radiation") demonstrate the effect of the irradiance distribution on the efficiency curve. The PTC

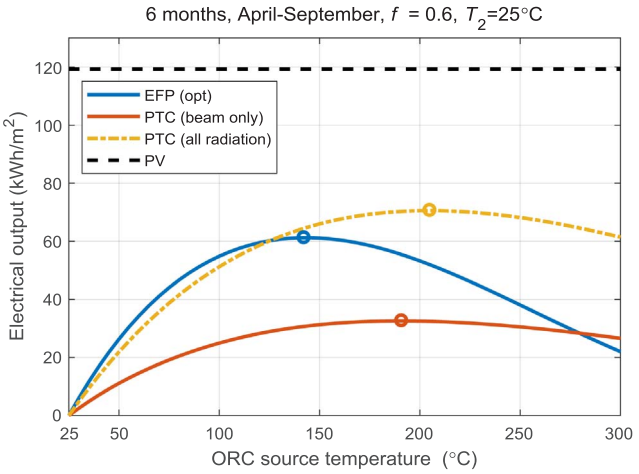

Fig. 13. Electrical energy output using solar collectors to power an Organic Rankine Cycle, compared with PV output, April–September.

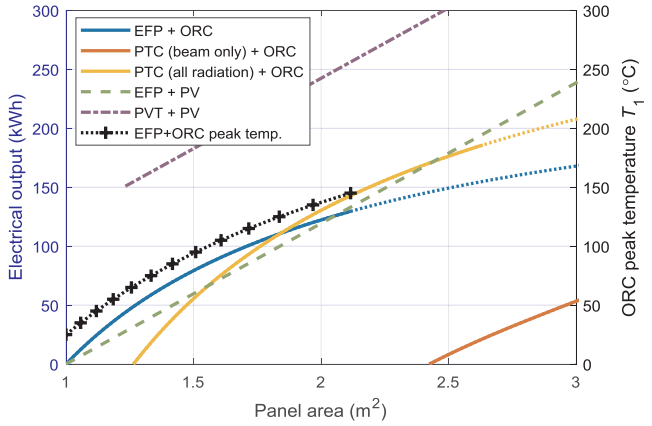

Fig. 14. Options for generating electrical power in addition to a six-monthly 623 kWh thermal output at 25 °C.

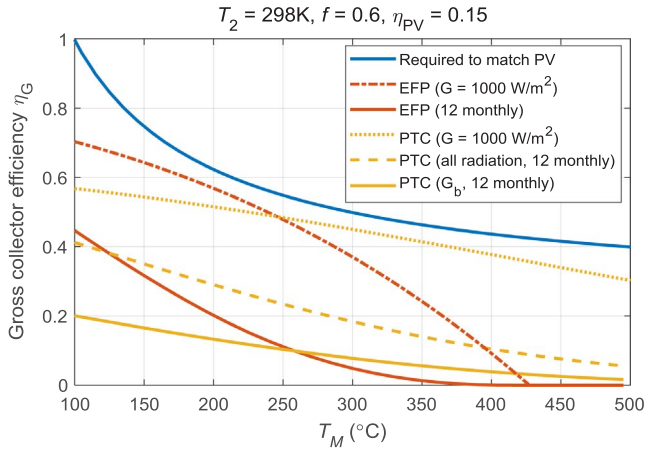

Fig. 15. Collector efficiencies that would be required in conjunction with an ORC to achieve the same electrical efficiency as a PV panel ("Required") compared with mean efficiencies under simulated conditions.

curve "G_b" shows the additional loss in efficiency under typical UK weather conditions because a concentrating collector can only focus and absorb beam radiation.

The "EFP + ORC" curve in Fig. 14 is lower than the "PVT + PV" because the annual mean efficiencies (Fig. 15) are less than half the clear sky G = 1000 W/m^2 efficiencies from Fig. 7(a).

6. Conclusions

An increase in efficiency equivalent to a reduction in heat loss coefficient U_L of 3.7 W/m^2 K has been observed when operating flat panel solar collectors under high vacuum.

The absorber used a flooded panel design with a black chrome plated coating. The coating emissivity was higher than intended. The resulting overall absorber heat loss coefficient U_L = 3.65 W/m^2 K was comparable to that available from the best non-evacuated commercial panels using high quality coatings. Simulations suggest that the loss coefficient could be reduced to U_L = 0.42 W/m^2 K (gross definition), 0.49 (absorber area) by combining a highly selective coating and a vacuum enclosure.

Simulations of the experimental tests closely modelled the measured efficiency.

Comparisons of efficiency data for flat plate, evacuated tube and parabolic trough solar collectors against a simulation using a high quality selective coating in an evacuated flat panel show that under high irradiance (G = 1000 W/m^2) the latter has an efficiency advantage for T_M < 210 °C. An evacuated flat plate at T_M = 60 °C can achieve an efficiency higher an evacuated tube by a factor of 1.32 and higher than a conventional flat panel by a factor of 1.13. At T_M = 100 °C there should be a 50% increase in heat output relative to either of these.

The high "medium temperature" efficiency of the evacuated plate collectors is well suited to process heat applications: at 117 °C delivery temperature the annual output from an optimised EFP is double the output from a parabolic trough collector. The efficiency claims for commercial evacuated panels by SRB and TVP are completely plausible and there may be some potential for further improvement in terms of coating emissivity. Given sufficient development and manufacturing investment, evacuated panels could eventually replace conventional flat plates and evacuated tubes for high efficiency applications.

The benefits of an evacuated flat plate collector become even more significant at lower irradiance levels. A simulation based on 6 years of weather data (Fig. 9, Table 5) showed that an evacuated flat plate collector could deliver 104% more heat to an 85 °C heating main than a conventional flat plate collector and 73% more than an evacuated tube collector. Transient modelling showed absorber heat capacity to have a significant effect in Winter but little effect on output during Summer months.

Domestic heating and hot water can use water temperatures as low as 40 °C if under-floor heating is employed. Below 58 °C the necessary panel area to meet a given Winter heating demand may be minimised by using a PVT panel plus heat pump combination instead of an evacuated flat plate (Fig. 10). There would be significant further advantages in terms of panel area if PV solar farms could be situated in a Mediterranean country with much higher levels of Winter insolation.

Comparing the annual value of both thermal and electrical outputs, evacuated thermal panels are preferable to the same area of PV or PVT panels when heat is required at temperatures above 70 °C (Fig. 11).

Thermal collectors can in principle drive an Organic Rankine Cycle to provide power as well as heat. Such systems were not cost-effective in terms of annual output compared with a combined PV/Thermal panel (Fig. 12). Annual heat output for each style of thermal collector is well fitted by a quadratic function of absorber temperature: this allows the peak output operating point for an Organic Rankine Cycle to be calculated.

Thermal collectors may be employed to charge a seasonal thermal store. When sized purely for the required thermal demand, an EFP requires less area than conventional collectors. If space permits, additional panel area can be used. This might be EFP collectors in association with an Organic Rankine cycle; EFP collector plus PV panels; or PVT and PV panels. For a 25 °C store in the UK, PVT panels require 23% more panel area than EFP collectors: if this is possible, a PVT-based system generates more electricity than any system using an EFP collector or an ORC (Fig. 14).

Under clear conditions with 1000 W/m^2 irradiance the output from an ORC coupled to either an EFP or a PTC would be approximately 9% less than obtained from a 15% efficiency PV panel of the same area (Fig. 15). Under UK weather conditions however the annual irradiance distribution (together with diffuse fraction in the PTC case) results in lower collector efficiencies and the use of an ORC becomes even less competitive.

Thermal collectors have a major role to play in the decarbonising of heat but not in electricity generation.

Acknowledgements

The authors are grateful to the Engineering and Physical Sciences Research Council (EPSRC) for funding this work as part of a collaborative programme between Warwick, Loughborough and Ulster universities, reference EP/K009915/1, EP/K010107/1 and EP/K009230/1. Matlab data and code used for the figures in this paper are openly available from http://wrap.warwick.ac.uk/id/eprint/89678.

Appendix A. Estimation of beam component

To allow use of incidence angle modifiers in the DIN CERTCO [69] dataset, the beam radiation component was estimated from the weather station's pyranometer readings using the following formulae from Duffie & Beckman [70]:

$I_{sc} = 1367\left(1 + 0.033\cos\left(\frac{2\pi \times n}{365}\right)\right)$ (W/m^2) where number n is the day of the year.

$\tau_b = a_o + a_1 e^{-k\sec\theta}$ where θ is the angle of the Sun from the zenith.

$\tau_d = 0.271-0.294\tau_b$

$G_{clear} = I_{sc}(\tau_b + \tau_d)$ is the expected instantaneous irradiance on a plane normal to the Sun's direction in clear weather.

An iterative scheme commencing with a nominal diffuse fraction $f_d = 0.5$ then identifies a combination of f_d and the clearness index k_T that would convert the clear sky irradiance G_{clear} at some angle ϕ away from the pyranometer axis into the observed irradiance G:

$$G = G_{clear}(f_d + (1-f_d)\cos\phi)k_T.$$

The correlation of Orgill and Hollands (Duffie) is used to relate k_T and f_d. An effective radiation level, including the incidence angle modifier $K_{\tau\alpha}$ for each collector, was then calculated as $G_E = G_d + G_b K_{\tau\alpha}\cos\phi$. Any ground-reflected component in the roof-mounted pyranometer reading was assumed to be negligible.

Appendix B. Transient collector response algorithm

The data analysis algorithm imports the data set for each month (t_i,$G_{E,i}$,$T_{a,i}$,i = 1: 44640) and predicts the absorber temperature and heat output for each minute using a time-marching scheme. The steady-state efficiency of each collector at G = 1000 W/m^2 was correlated as a cubic formula, Eq. (1), from which the output at lower light levels could be calculated:

$$Q_{in,i} = G_{E,i}\eta_0-(\alpha_1 T_{M,i} + \alpha_2 T_{M,i}^2 + \alpha_3 T_{M,i}^3) \quad (6)$$

This heat flux if positive is delivered to the heating main once the absorber has reached the heating main temperature T_{HM}. The analysis assumed that the heat transfer fluid would be pumped whenever the net heat output was positive and turned off at other times; when pumped, the fluid would be limited to the heating main temperature (taken for simplicity as a constant, T_{HM} = 85 °C). While G is below the critical level (whether over-night or during a period of poor light) the model predicts absorber temperature to determine when the next heat delivery period begins.

For simplicity, Eq. (6) was linearised in terms of a tangent $Q_i = (G_E\eta'_0)_i-U'_L T_{M,i}$ to the (T_M,Q_{in}) curve at each time step. The first order lumped capacity model for periods with the pump switched off is then:

$$C\frac{\mathrm{d}T}{\mathrm{d}t} = (G_E\eta'_0)_i-U'_{L,i}(T-T_{a,i}) \quad (7)$$

and has solutions over each 60 s period between weather data readings of the form $T = T_{asymp} + (T_i-T_{asymp})e^{-\lambda t}$ where $\lambda = \frac{U_{L,i}}{C}$, $T_{assymp} = \frac{(G_E\eta_0)_i}{U_{L,i}} + T_{a,i}$.

C is the short-term heat capacity (J/m^2 K) of the absorber under no-flow conditions and has been estimated from typical dimensions and fluid capacity. For simplicity the mass of any cover glass has been omitted since this is not in direct thermal contact with the absorber.

This models allows the prediction of the complete absorber temperature profile for each month, starting from the assumption $T_1 = T_{a,1}$ at midnight for the first dataset point. Solution of Eq. (7) gives the absorber temperatures for $i > 1$:

$$T_{i+1} = \min[T_{HM}, T_{asymp,i} + (T_i-T_{asymp,i})e^{-60\lambda}].$$

The heat input to the district heating main over each time step is:

$$E_{u,i} = \max(0, Q_{u,i}\Delta t_i)$$

$E_{u,i}$ is positive when G_i exceeds the critical radiation level provided that the absorber temperature T_i is not below the heating main temperature T_{HM}. The effective time period Δt_i was calculated for intervals where the switching on or off of the pump due to changing temperature or insolation brought the heat transfer period below the nominal 60 s.

References

[1] DTI, Energy consumption in the United Kingdom; 2001 < http://webarchive.nationalarchives.gov.uk/ + /http:/www.berr.gov.uk/files/file11250.pdf > .

[2] Kalogirou SA. Solar Energy Engineering. 2nd ed. Academic Press; 2014.

[3] Riggs BC, Biedenharn R, Dougher C, Ji YV, Xu Q, Romanin V, et al. Techno-economic analysis of hybrid PV/T systems for process heat using electricity to subsidize the cost of heat. Appl Energy 2017;208:1370–8.

[4] Alam M, Singh H, Suresh S, Redpath DAG. Energy and economic analysis of Vacuum Insulation Panels (VIPs) used in non-domestic buildings. Appl Energy 2017;188:1–8.

[5] Leone G, Beccali M. Use of finite element models for estimating thermal performance of façade-integrated solar thermal collectors. Appl Energy 2016;171:392–404.

[6] O'Hegarty R, Kinnane O, McCormack SJ. Concrete solar collectors for façade integration: an experimental and numerical investigation. Appl Energy 2017;206:1040–61.

[7] Moss RW, Henshall P, Arya F, Shire GSF, Eames PC, Hyde T. Simulator testing of evacuated flat plate solar collectors for industrial heat and building integration. Solar Energy 2017. submitted for publication.

[8] Suman S, Khan MK, Pathak M. Performance enhancement of solar collectors – a review. Renew Sustain Energy Rev 2015;49:192–210.

[9] Colangelo G, Favale E, Miglietta P, de Risi A. Innovation in flat solar thermal collectors: a review of the last ten years' experimental results. Renew Sustain Energy Rev 2016;57:1141–59.

[10] Selvakumar N, Barshilia HC. Review of physical vapor deposited (PVD) spectrally selective coatings for mid- and high-temperature solar thermal applications. Sol Energy Mater Sol Cells 2012;98:1–23.

[11] Colangelo G, Favale E, Miglietta P, de Risi A, Milanese M, Laforgia D. Experimental test of an innovative high concentration nanofluid solar collector. Appl Energy 2015;154:874–81.

[12] Caër VH-L, De Chambriera E, Mertina S, Jolya M, Schaerb M, Scartezzinia J-L. Optical and morphological characterisation of low refractive index materials for coatings on solar collector glazing. Renew Energy May 2013;53:27–34.

[13] Freeman J, Hellgardt K, Markides CN. An assessment of solar-thermal collector designs for small-scale combined heating and power applications in the United Kingdom. Heat Transfer Eng 2015;36(14–15). http://dx.doi.org/10.1080/01457632.2015.995037.

[14] Nkwetta DN, Smythe M. The potential applications and advantages of powering solar air-conditioning systems using concentrator augmented solar collectors. Appl Energy 2012;89:380–6.

[15] Alobaid M, Hughes B, Calautit JK, O'Connor D, Heyes A. A review of solar driven absorption cooling with photovoltaic thermal systems. Renew Sustain Energy Rev 2017;76:728–42.

[16] Bouvier J-L, Michaux G, Salagnac P, Kientz T, Rochier D. Experimental study of a micro combined heat and power system with a solar parabolic trough collector

coupled to a steam Rankine cycle expander. Sol Energy 2016;134:180–92.
[17] Purohit I, Purohit P. Technical and economic potential of concentrating solar thermal power generation in India. Renew Sustain Energy Rev 2017;78:648–66.
[18] Zou B, Dong J, Yao Y, Jiang Y. An experimental investigation on a small-sized parabolic trough solar collector for water heating in cold areas. Appl Energy 2016;163:396–407.
[19] Cohen S, Grossman G. Development of a solar collector with a stationary spherical reflector/tracking absorber for industrial process heat. Sol Energy 2016;128:31–40.
[20] Buttinger F, Beikircher T, Proll M, Scholkopf W. Development of a new flat stationary evacuated CPC-collector for process heat applications. Sol Energy 2010;84:1166–74.
[21] Wang J, Yin Z, Qi J, Ma G, Liu X. Medium-temperature solar collectors with all-glass solar evacuated tubes. Energy Procedia 2015;70:126–9.
[22] Li Q, Zheng C, Shirazi A, Mousa OB, Moscia F, Scott JA. Design and analysis of a medium-temperature, concentrated solar thermal collector for air-conditioning applications. Appl Energy 2017;190:1159–73.
[23] Mwesigye A, Meyer JP. Optimal thermal and thermodynamic performance of a solar parabolic trough receiver with different nanofluids and at different concentration ratios. Appl Energy 2017;193:393–413.
[24] Qu W, Wang R, Hong H, Sun J, Jin H. Test of a solar parabolic trough collector with rotatable axis tracking. Appl Energy 2017. [in press].
[25] Benz N, Beikircher T. High efficiency evacuated flat-plate solar collector for process steam production. Sol Energy 1999;65(2):111–8.
[26] Beikircher T, Möckl M, Osgyan P, Streib G. Advanced solar flat plate collectors with full area absorber, front side film and rear side vacuum superinsulation. Sol Energy Mater Sol Cells 2015;141:308–406.
[27] Ehrmann N, Reineke-Koch R. Selectively coated high efficiency glazing for solar-thermal flat-plate collectors. Thin Solid Films 2012;520:4214–8.
[28] Brunold S, Frey R, Frei U. A comparison of three different collectors for process heat applications. SPF publication < http://spf.ch/fileadmin/daten/publ/procheat.pdf>.
[29] Benvenuti C, Ruzinov V. The SRB evacuated flat solar panel. In: Proceedings of ECOS, 2010, p. 2-429 –434.
[30] Benvenuti C. The SRB solar thermal panel. Europhys News 2013:16–8. http://dx.doi.org/10.1051/epn/2013301.
[31] Benvenuti C. Particle accelerators and solar panels. Fisica E 2013;29(1–2):31–8. (NEG Non-evaporable getters etc).
[32] Abbate P. Presentation on the TVP evacuated panel at InterSolar 2012 < https://www.youtube.com/watch?v=z_4FD4Zxwew> [accessed 12/7/2017].
[33] TVP Solar, MT-30 datasheet < http://www.tvpsolar.com/files/pagine/1464011780_MT-Power%20Datasheet%20(v4.2x)(ver5).pdf> [accessed 12/7/2017].
[34] Henshall P, Moss R, Arya F, Eames PC, Shires S, Hyde T. An evacuated enclosure design for solar thermal energy applications. Grand Renewable Energy 2014 (GRE2014) International Conference and Exhibition, Tokyo, Japan, 27 July–1 August 2014 < https://dspace.lboro.ac.uk/2134/16098 > .
[35] SPF catalogue of solar collector test results < http://www.spf.ch/index.php?id=111&L=6> [accessed August 2017].
[36] Moss RW, Shire GSF, Henshall P, Eames PC, Arya F, Hyde T. Optimal passage size for solar collector micro-channel and tube-on-plate absorbers. Sol Energy 2017;153:718–31. http://dx.doi.org/10.1016/j.solener.2017.05.030.
[37] Moss RW, Shire GSF, Henshall P, Eames PC, Arya F, Hyde T. Design and fabrication of a hydro-formed absorber for an evacuated solar collector. Appl Therm Eng 2017. Submitted for publication.
[38] Lira-Cantú M, Sabio AM, Brustenga A, Gómez-Romero P. Electrochemical deposition of black nickel solar absorber coatings on stainless steel AISI316L for thermal solar cells. Sol Energy Mater Sol Cells 2005;87:685–94.
[39] Lizama-Tzec FI, Macías JD, Estrella-Gutiérrez MA, Cahue-López AC, Arés O, de Coss R, et al. Electrodeposition and characterization of nanostructured black nickel selective absorber coatings for solar–thermal energy conversion. J Mater Sci : Mater Electron 2015;26:5553–61. http://dx.doi.org/10.1007/s10854-014-2195-5.
[40] Joly M, Antonetti Y, Python M, Gonzalez M, Gascou T, Scartezzini J-L, et al. Novel black selective coating for tubular solar absorbers based on a sol–gel method. Sol Energy 2013;94:233–9.
[41] Gao X-H, Theiss W, Shen Y-Q, Ma P-J, Liu G. Optical simulation, corrosion behavior and long term thermal stability of TiC-based spectrally selective solar absorbers. Sol Energy Mater Sol Cells 2017;167:150–6.
[42] McDonald GE. Spectral reflectance properties of black chrome for use as a solar selective coating. Sol Energy 1975;17:119–22.
[43] Moss RW, Shire GSF, Eames PC, Henshall P, Hyde T, Arya F. Design and commissioning of a virtual image solar simulator for testing thermal collectors. Sol Energy 2017;159:234–42. http://dx.doi.org/10.1016/j.solener.2017.10.044. January 2018.
[44] Thorpe, University of Warwick Weather Station (online) < https://www2.warwick.ac.uk/fac/cross_fac/sciencecity/programmes/internal/themes/energyefficiency/thermal/bookings/weather_station/ > [accessed October 2017].
[45] Matuska T, Sourek B, Jirka V, Pokorny N. Glazed PVT collector with polysiloxane encapsulation of PV cells: performance and economic analysis. Int J Photoenergy 2015. http://dx.doi.org/10.1155/2015/718316.
[46] NEP PolyTrough 1800 datasheet accessed August 2017 < http://www.nep-solar.com/wp-content/uploads/2013/11/NEP-Solar-Polytrough1800_Datasheet.pdf > .
[47] Zambolin E, Col DD. Experimental analysis of thermal performance of flat plate and evacuated tube solar collectors in stationary standard and daily conditions. Sol Energy 2010;84:1382–96.
[48] Zima W, Dziewa P. Modelling of liquid flat-plate solar collector operation in transient states. In: Proc. IMechE Vol. 225 Part A (2010) J. Power and Energy pp 53–62.
[49] Rodríguez-Hidalgo MC, Rodríguez-Aumente PA, Lecuona A, Gutiérrez-Urueta GL, Ventas R. Flat plate thermal solar collector efficiency: Transient behavior under working conditions. Part I: model description and experimental validation. Appl Therm Eng 2011;31:2394–404.
[50] Amrizal N, Chemisana D, Rosell JI. Hybrid photovoltaic–thermal solar collectors dynamic modelling. Appl Energy 2013;101:797–807.
[51] Gao Y, Zhang Q, Fan R, Lin X, Yu Y. Effects of thermal mass and flow rate on forced-circulation solar hot-water system: comparison of water-in-glass and U-pipe evacuated-tube solar collectors. Solar Energy 2013;98:290–301.
[52] Agrawal S, Tiwari GN. Energy and exergy analysis of hybrid micro-channel photovoltaic thermal module. Sol Energy 2011;85:356–70.
[53] RISE, ScenoCalc home page < http://www.sp.se/en/index/services/solar/ScenoCalc/Sidor/default.aspx > [accessed December 2017].
[54] Evinox data sheet (downloaded 28/11/2017): < http://www.evinoxenergy.co.uk/Sites/Evinox/library/files/PHRIE%20ASHP%20Data%20Sheet.pdf > .
[55] Palz W, Greif J. Commission of the European communities. European solar radiation atlas. 3d ed. Springer; 1996. p. 326.
[56] Ancona MA, Bianchi M, Diolaiti E, Giannuzzi A, Marano B, Melino F, Peretto A. A novel solar concentrator system for combined heat and power application in residential sector. Appl Energy 2017;185:1199–209.
[57] Crisostomo F, Hjerrild N, Mesgari S, Li Q, Taylor RA. A hybrid PV/T collector using spectrally selective absorbing nanofluids. Appl Energy 2017;193:1–14.
[58] Modjinou M, Ji J, Li J, Yuan W, Zhou F. A numerical and experimental study of micro-channel heat pipe solar photovoltaics thermal system. Appl Energy 2017;206:708–22.
[59] Bianchini A, Guzzini A, Pellegrini M, Saccani C. Photovoltaic/thermal (PV/T) solar system: experimental measurements, performance analysis and economic assessment. Renew Energy 2017;111:543–55.
[60] Herrando M, Markides C. Hybrid PV and solar-thermal systems for domestic heat and power provision in the UK: techno-economic considerations. Appl Energy 2016;161:512–32.
[61] Abdelhamid M, Widyolar BK, Jiang L, Winton R, Yablonovitch E, Scranton G, et al. Novel double-stage high-concentrated solar hybrid photovoltaic/thermal (PV/T) collector with nonimaging optics and GaAs solar cells reflector. Appl Energy 2016;182:68–79.
[62] Lee D-S, Hung T-C, Lin J-R, Zhao J. Experimental investigations on solar chimney for optimal heat collection to be utilized in organic Rankine cycle. Appl Energy 2015;154:651–62.
[63] Quoilin S, Orosz M, Hemond H, Lemort V. Performance and design optimization of a low-cost solar organic Rankine cycle for remote power generation. Sol Energy 2011;85:955–66.
[64] Landelle A, Tauveron N, Haberschill P, Revellin R, Colasson S. Organic Rankine cycle design and performance comparison based on experimental database. Appl Energy 2017;204:1172–87.
[65] Su W, Zhao L, Deng S, Xu W, Yu Z. A limiting efficiency of subcritical Organic Rankine cycle under the constraint of working fluids. Energy 2018;143:458–66.
[66] Rad FM, Fung AS. Solar community heating and cooling system with borehole thermal energy storage – review of systems. Renew Sustain Energy Rev 2016;60:1550–61.
[67] Chapuis S, Bernier M. Seasonal storage of solar energy in borehole heat exchangers. In: Proc. 11th International Building Performance Simulation Association (IBPSA) meeting 2009, Glasgow, 599–606.
[68] Busby J. UK shallow ground temperatures for ground coupled heat exchangers. Q J Eng Geol Hydrogeol 2015;48:248–60. https://0-doi-org.pugwash.lib.warwick.ac.uk/10.1144/qjegh2015-077.
[69] DIN CERTCO test certificates < http://www.dincertco.tuv.com > [accessed August 2017].
[70] Duffie JA, Beckman WA. Solar Engineering of Thermal Processes. 4th ed. Wiley; 2013.